This is a "preproof" accepted article for *Mineralogical Magazine*.
This version may be subject to change during the production process.
10.1180/mgm.2025.8

Revision 1
Badalovite, $NaNaMg(MgFe^{3+})(AsO_4)_3$, and associated calciojohillerite, $NaCaMgMg_2(AsO_4)_3$, from Biancavilla, Etna volcanic complex, Sicily, (Italy): occurrence and crystal chemistry

DANIELA MAURO[1,2*], JIŘÍ SEJKORA[3], and ZDENĚK DOLNÍČEK[3]

[1]*Museo di Storia Naturale, Università di Pisa, Via Roma 79, 56011 Calci (PI), Italy*
[2]*Dipartimento di Scienze della Terra, Università di Pisa, Via Santa Maria 53, 56126 Pisa, Italy*
[3]*Department of Mineralogy and Petrology, National Museum, Cirkusová 1740, 193 00 Praha 9, Czech Republic*
e-mail address: daniela.mauro@unipi.it*

ABSTRACT

Two alluaudite-group minerals, badalovite, ideally $NaNaMg(MgFe^{3+})(AsO_4)_3$, and calciojohillerite, $NaCaMgMg_2(AsO_4)_3$, have been identified on a specimen from the Monte Calvario quarry, Biancavilla, Etna volcanic complex, Sicily, Italy. For both species, this finding represents the second world occurrence. The studied sample was characterized using electron microprobe analysis, micro-Raman spectroscopy, and single-crystal X-ray diffraction. Badalovite occurs as vitreous to resinous aggregates of yellowish to brownish prismatic crystals, up to 0.5 mm in length, associated with tabular crystals of hematite, pseudobrookite, and an amphibole-supergroup mineral. Badalovite is intimately intergrown with minor calciojohillerite. The chemical formulae of these two alluaudite-group members, recalculated on the basis of 12 O atoms per formula unit and assuming the occurrence of Fe^{3+}, are $(Na_{1.74(11)}K_{0.01(1)}Ca_{0.30(8)})_{\Sigma 2.05}$ $(Mg_{1.74(2)}Mn_{0.27(2)}Ca_{0.11(8)}Zn_{0.03(1)}Fe_{0.84(14)}Al_{0.02(2)})_{\Sigma 3.01}$ $(As_{2.85(4)}P_{0.11(3)})_{\Sigma 2.96}$ O_{12} and $(Na_{1.44(2)}K_{0.01(1)}Ca_{0.66(1)})_{\Sigma 2.11}$ $(Mg_{2.27(1)}Mn_{0.28(1)}Zn_{0.01(1)}Fe_{0.48(2)})_{\Sigma 3.00}$ $(As_{2.79(3)}P_{0.13(2)})_{\Sigma 2.92}$ O_{12}, respectively. Single crystal X-ray diffraction data collected on badalovite gave the following unit-cell parameters a = 11.9760(5), b = 12.7857(5), c = 6.6650(3) Å, β = 112.689(2)°, V = 941.58(7) Å^3, space group $C2/c$. Its crystal structure was refined to R_1 = 0.0257 for 1711 unique reflections with $F_o > 4\sigma(F_o)$ and 97 least-square parameters. The crystal chemical and spectroscopic data as well as the genesis of badalovite are discussed and a comparison with the Russian type material is reported.

https://doi.org/10.1180/mgm.2025.8 Published online by Cambridge University Press

Keywords: badalovite, calciojohillerite, alluaudite group, arsenate, crystal chemistry, Raman spectroscopy, Monte Calvario quarry, Etna volcanic complex, Sicily, Italy.

Introduction

The alluaudite supergroup includes phosphate and arsenate minerals characterized by monoclinic symmetry, space group $C2/c$ or $P2_1/n$, and by unit-cell parameters $a \sim 12$, $b \sim 12.5$, $c \sim 6.5$ Å, $\beta \sim 115°$ (Hatert, 2019; Tait *et al*., 2021). The general formula of the members of the alluaudite supergroup is $A(2)'A(1)M(1)M(2)_2(TO_4)_3$, [where A = Na, Ca, Cu^{2+} or □; M = Mn^{2+}, Fe^{3+}, Fe^{2+}, Mg, Al, Cu^{2+}, Zn, Cd, Ca or Na; T = P or As (Hatert, 2019; Tait *et al*., 2021)]. This supergroup is divided into four groups, i.e., the alluaudite-, wyllieite-, bobfergusonite-, and manitobaite-group. All the members of these groups are characterized by the same topology and they can be identified on the basis of different cation-ordering schemes at the octahedral sites (Hatert, 2019; Tait *et al*., 2021). The alluaudite group, mainly formed by arsenate minerals, contains the largest number of species.

Arsenates are usually supergene minerals related to the weathering of As-bearing ores (e.g., As-rich pyrite, arsenopyrite, As-bearing sulfosalts). However, other geological environments can be characterized by the occurrence of arsenate minerals (e.g., Auernhammer *et al*., 1993; Majzlan *et al*., 2014, Pekov *et. al*., 2018, Hatert, 2019, Tait *et al*., 2021). An intriguing mineral assemblage has been discovered at the active Arsenatnaya fumarole, Second scoria cone, Tolbachik Volcanic field, Kamchatka Peninsula, Russia, where more than fifty arsenates have been identified so far. Among them, fortysix are still endemic, and ten of them allowed the description of novel crystal structures (Pekov *et. al*., 2018). The most common arsenate minerals occurring at the Arsenatnaya fumarole belong to the alluaudite group and nine have there their type locality, i.e., badalovite (Pekov *et al*., 2020a), calciojohillerite (Pekov *et al*., 2021), calciohatertite (Koshlyakova *et al*., 2021), hatertite (Krivovichev *et al*., 2013), khrenovite (Pekov *et al*., 2022a), magnesiohatertite (Pekov *et al*., 2016), manganobadalovite (Koshlyakova *et al*., 2020), manganohatertite (Koshlyakova *et al*., 2024), and paraberzeliite (Pekov *et al*., 2022b). All of them are endemic.

During the 45th Sicily Mineral Show, in November 2023, a specimen from the Monte Calvario quarry (Biancavilla, Etna volcanic complex, Sicily, Italy) was given to one of us (D.M.) by the mineral collector Gaetano Sicurella in order to investigate an unknown phase previously reported as "Unnamed Mineral (UM2)", chemically characterized by the occurrence of major Na and As, with minor Fe, P, and Ca (Sicurella *et al*., 2010). The Monte Calvario quarry is well-known for being the type locality for two F-bearing phases, i.e., fluoro-edenite and fluorophlogopite (Gianfagna and Oberti, 2001; Gianfagna *et al*., 2007a). A review of the geological, volcanological, mineralogical, and environmental features of the Monte Calvario area can be found in Burragato *et al*. (2005). This area was interpreted by these authors as a locally metasomatized benmoreitic lava dome and dyke complex with associated autoclastic breccias.

This paper aims to provide further data on badalovite and associated calciojohillerite based on the data collected on this new Italian occurrence, representing the second world finding of these alluaudite-group minerals.

https://doi.org/10.1180/mgm.2025.8 Published online by Cambridge University Press

Experimental

Studied specimen

In the hand specimen, the studied sample is characterized by a fragment of altered benmoreitic rock, 2.5 × 1.5 × 1.7 cm in size, characterized by cavities, up to 1 cm across. The walls of the cavities are covered by vitreous to resinous yellowish to brownish prismatic crystals, in some cases forming sheaf-like aggregates up to 0.5 mm in length, associated with equant to tabular crystals of hematite (Fig. 1). Other associated minerals are pseudobrookite and an amphibole-supergroup mineral (probably fluoro-edenite). The grains used for single crystal X-ray diffraction are deposited in the mineralogical collection of the Museo di Storia Naturale of the Università di Pisa, under catalogue number 20080; one grain, used for quantitative chemical analyses, is stored in the mineralogical collection of the National Museum, Prague, under the catalogue number P1P 55/2024.

Chemical analysis

An orange-brownish prismatic crystal was sampled from the studied specimen in order to perform electron microprobe analyses. Quantitative chemical analyses were collected at the National Museum of Prague (Czech Republic), using a Cameca SX100 electron microprobe. The following analytical conditions were used: WDS mode, accelerating voltage 15 kV, beam current 5 nA, beam size 10 μm. The following standards (element, emission line) were used: celestine (S*K*α), fluorapatite (Ca*K*α, P*K*α), clinoclase (As*L*α), sanidine (Al*K*α, K*K*α), hematite (Fe*K*α), diopside (Mg*K*α), rhodonite (Mn*K*α), ZnO (Zn*K*α), and albite (Na*K*α). Fluorine, Si, Cl, Co, and Pb were sought but found below the detection limit. Peak counting times were 20 s on the peak and 10 s on each background. Matrix correction by PAP algorithm (Pouchou and Pichoir, 1985) and automatic corrections of overlaps Ca-P and Na-Zn were applied to the data. Quantitative chemical data and the empirical chemical formulae are given in Table 1.

Micro-Raman spectroscopy

Micro-Raman spectra of badalovite were collected, in the range between 100-4000 cm^{-1}, on the same grain used for single crystal X-ray diffraction and for electron microprobe analyses in WDS mode using a Horiba Jobin-Yvon XploRA Plus apparatus, equipped with a motorized *x-y* stage and an Olympus BX41 microscope with a 50× objective (Dipartimento di Scienze della Terra, Università di Pisa). Raman spectra were excited using a 532 nm line of a solid-state laser, attenuated to 25% (*i.e.*, 6.25 mW). The minimum lateral and depth resolution was set to a few μm. The system was calibrated using the 520.6 cm^{-1} Raman band of silicon before each experimental session. Spectra were collected through multiple acquisitions (3) with counting time of 80 s. Backscattered radiation was analyzed with a 1200 gr/mm grating monochromator. Experimental precision can be estimated at ± 2 cm^{-1}. The thermal damage of the measured points was excluded by the visual inspection of the excited surface after measurement, by the observation of the possible decay of spectral features in the start of excitation and checking for thermal downshift of Raman lines. Raman spectra were processed

https://doi.org/10.1180/mgm.2025.8 Published online by Cambridge University Press

using *Fityk* (Wojdyr, 2010). Table 2 gives the position of observed bands and their possible interpretation.

X-ray crystallography

Single-crystal X-ray diffraction (SCXRD) data for badalovite were collected using a Bruker D8 Venture diffractometer (50 kV, 1.4 mA) equipped with an air-cooled Photon III detector, and a microfocus Mo*K*α radiation (Centro per l'Integrazione della Strumentazione scientifica dell'Università di Pisa, University of Pisa, Italy). The detector-to-crystal distance was set to 38 mm. Data were collected using φ and ω scan modes, in 0.5° slices. Intensity data were integrated and corrected for Lorentz, polarization, background effects, and absorption using the package of software APEX4 (Bruker AXS Inc., 2022). Badalovite is monoclinic, space group *C*2/*c*, with unit-cell parameters: a = 11.9760(5), b = 12.7857(5), c = 6.6650(3) Å, β = 112.689(2)°, V = 941.58(7) Å^3. Crystal structure refinement was performed using Shelxl-2018 (Sheldrick, 2015) starting from the atomic coordinates given by Pekov *et al.* (2020a). Taking into account the results of chemical analysis, the following neutral scattering curves were used from the *International Tables for Crystallography* (Wilson, 1992): Na *vs*. Ca at the *A*(1); Na at *A*(2)' sites; Mg *vs*. Mn at the *M*(1) site; Mg *vs*. Fe at the *M*(2) site; As *vs*. P at the *T* site; and O at O(1) – O(6) sites. Several cycles of isotropic refinement converged to R_1 = 0.0439, thus confirming the correctness of the structural model. After the modelling of the anisotropic displacement parameters of cations only, the R_1 was lowered to 0.0297, further lowered to 0.0254 after the introduction of anisotropic displacement parameters also for O sites. At this step of refinement, the As/(As+P) ratio at the two independent *T* sites was 0.898, to be compared with a value of 0.96 measured through electron microprobe data (see below). Because the average <*T*–O> distances do not suggest a significant P content, it was preferred to fix the As and P content at the *T*(1) and *T*(2) sites in accord with the site occupancies calculated on the basis of the observed average bond distances and the <As–O> and <P–Φ> (where Φ = O, OH) grand values given by Majzlan *et al*. (2014) and Huminicki and Hawthorne (2002), respectively. The crystal structure refinement converged to R_1 = 0.0257 for 1637 unique reflections with $F_o > 4\sigma(F_o)$ and 97 least-square parameters.

In Table 3, details of data collection and crystal structure refinement are reported. Atomic coordinates and equivalent isotropic displacement parameters are given in Table 4. The selected bond distances of badalovite are reported in Table 5. Bond valence sums (BVS), calculated using the bond parameters of Gagné and Hawthorne (2015) and taking into account the proposed site populations, are given in Table 6. The Crystallographic Information File (CIF) of badalovite is available as Supplementary Material.

Results and discussion

Chemical data

X-ray elemental maps (Fig. 2) revealed, within the studied grain, the occurrence of an inner portion enriched in Na and Fe and depleted in Ca, whereas crystal rims are enriched in Ca and Mg, with a detectable depletion in Fe. The bond distances and the bond valence sums for the *M*(2) site (see below) strongly support the occurrence of iron as Fe^{3+}, in agreement with the oxidized nature of the mineral assemblage, as suggested by the occurrence of

https://doi.org/10.1180/mgm.2025.8 Published online by Cambridge University Press

hematite and pseudobrookite, as well as the results of Mössbauer study on fluoro-edenite by Gianfagna *et al*. (2007b) and Andreozzi *et al*. (2009). The observed element distribution agrees with the heterovalent substitution $Na^{+} + Fe^{3+} = Ca^{2+} + Mg^{2+}$.

Table 1 reports the chemical analyses of the studied grain and the chemical formulae corresponding to the ten spot analyses, recalculated on the basis of 12 O atoms per formula unit (apfu). Defining ΣM as the sum of all octahedrally-coordinated cations and ΣA as the sum of the chemical constituents at the *A*(1) and *A*(2)' sites, Figure 3 shows the relation between $M^{2+}/\Sigma M$ (where M^{2+} is the sum of divalent octahedral cations) and $A^{+}/\Sigma A$ (where A^{+} is the sum of Na and minor K). It becomes clear that three chemical domains occur, corresponding to the following average chemical formulae:

I) $(Na_{1.82(11)}K_{0.01(1)}Ca_{0.24(8)})_{\Sigma 2.07}$ $(Mg_{1.57(2)}Mn_{0.28(2)}Ca_{0.13(8)}Zn_{0.03(1)}Fe_{0.93(14)}Al_{0.02(2)})_{\Sigma 3.00}$ $(As_{2.87(4)}P_{0.09(3)})_{\Sigma 2.96}O_{12}$;

II) $(Na_{1.62(11)}Ca_{0.49(8)})_{\Sigma 2.11}$ $(Mg_{2.02(2)}Mn_{0.27(2)}Zn_{0.02(1)}Fe_{0.68(14)}Al_{0.01(2)})_{\Sigma 3.00}$ $(As_{2.80(4)}P_{0.11(3)})_{\Sigma 2.91}O_{12}$;

III) $(Na_{1.44(2)}K_{0.01(1)}Ca_{0.66(1)})_{\Sigma 2.11}$ $(Mg_{2.27(1)}Mn_{0.28(1)}Zn_{0.01(1)}Fe_{0.48(2)})_{\Sigma 3.00}$ $(As_{2.79(3)}P_{0.13(2)})_{\Sigma 2.92}O_{12}$.

The first domain shows a chemical composition near to the end-member formula of badalovite, i.e., $^{A(1)}Na^{A(2)'}Na^{M(1)}Mg^{M(2)}(MgFe^{3+})(AsO_4)_3$. However, minor chemical substitutions were identified in the studied sample with respect to the ideal composition. These chemical variations are in agreement with the known crystal chemistry of the alluaudite-group minerals (e.g., Hatert, 2019). The occurrence of Mn, Zn, and Ca in arsenate members of the alluaudite group was found in several species as, for instance, in zincobradaczekite, caryinite, and arseniopleite (Pekov *et al*., 2020b; Ercit, 1993; Tait and Hawthorne, 2003).

The second domain has still an end-member formula corresponding to that of badalovite, even if its content of calciojohillerite component is higher, with an empirical composition very close to the boundary between the two species. Finally, the remaining two spot analyses (third domain), correspond to the end-member formula of calciojohillerite, $^{A(1)}Na^{A(2)'}Ca^{M(1)}Mg^{M(2)}Mg_2(AsO_4)_3$.

Figure 2 clearly shows that domains I and II are the most abundant in the studied grain. For this reason, the average composition of spots 1-8 is considered as representative of the average chemistry of the crystal investigated through single-crystal X-ray diffraction, i.e., $(Na_{1.74(11)}K_{0.01(1)}Ca_{0.30(8)})_{\Sigma 2.05}(Mg_{1.74(2)}Mn_{0.27(2)}Ca_{0.11(8)}Zn_{0.03(1)}Fe_{0.84(14)}Al_{0.02(2)})_{\Sigma 3.01}(As_{2.85(4)}P_{0.11(3)})_{\Sigma 2.96}O_{12}$, thus corresponding to badalovite. Comparing the average chemistry of the studied sample with those of the Russian badalovite, the Italian one shows higher Mn content as well as minor enrichment in Ca, Na and P [i.e., *A* = $(Na_{1.74(11)}K_{0.01(1)}Ca_{0.30(8)})_{\Sigma 2.05}$ *vs.* $(Na_{1.67}K_{0.02}Ca_{0.20})_{\Sigma 1.89}$, *M* = $(Mg_{1.74(2)}Mn_{0.27(2)}Ca_{0.11(8)}Zn_{0.03(1)}Fe_{0.84(14)}Al_{0.02(2)})_{\Sigma 3.01}$ *vs.* $(Mg_{1.92}Mn_{0.02}Cu_{0.1}Zn_{0.02}Fe_{0.90})_{\Sigma 2.87}$ and *T* = $(As_{2.85(4)}P_{0.11(3)})_{\Sigma 2.96}$ *vs.* $(As_{3.01}P_{0.03}Si_{0.01})_{\Sigma 3.05}$, respectively].

https://doi.org/10.1180/mgm.2025.8 Published online by Cambridge University Press

Micro-Raman spectroscopy

The micro-Raman spectrum of badalovite is characterized by the occurrence of the four fundamental modes of $(AsO_4)^{3-}$ groups, by the vibration modes of the *A*– and *M*–O cations hosted in its crystal structure as well as to lattice vibration modes (Figure 4). Three spectral ranges can be recognized, in agreement with the previous data (Pekov *et. al*., 2020a), i.e., between 100-300 cm^{-1}, 300-600 cm^{-1}, and between 750-950 cm^{-1}. The strongest Raman bands occur in the latter region and are related to the symmetric (v_1) and antisymmetric (v_3) stretching modes of the $(AsO_4)^{3-}$ groups (e.g., Sejkora *et al*., 2020).The arsenate bending modes (v_2 and v_4) occur in the range between 300-570 cm^{-1} (e.g., Sejkora *et al*., 2020). Raman bands below to 300 cm^{-1} can be attributed to the vibration modes of the *A*– and *M*–O cations as well as to the lattice vibration modes (Pekov *et. al*., 2020a; Pekov *et. al*., 2021; Sejkora *et al*., 2020). Raman bands of Italian and Russian badalovite as well as of Russian calciojohillerite are given in Table 2. In agreement with the isotypic relationship occurring between the last two member of the alluaudite-group minerals they show similar Raman spectra. Minor differences between badalovite and calciojohillerite spectra could be interpreted as a consequence of chemical changes (e.g., below 300 cm^{-1}), as well as to the methods used for the identification of the band positions. Moreover, in agreement with the previous data, no bands due to the occurrence of H_2O groups were observed in the O–H bending or stretching regions. Finally, no evidence of vibration modes due to the occurrence of $(AsO_3OH)^{2-}$ groups occurs (e.g., Sejkora *et al*., 2020).

Crystal structure description

The crystal structure of badalovite, in agreement with the previous study by Pekov *et al*. (2020a), is composed by zig-zag chains, running along [10-1], formed by edge-sharing $[M(2)_2O_{10}]$ dimers connected through distorted $M(1)O_6$ octahedra. Adjacent chains are connected through corner-sharing of $T(1)O_4$ tetrahedra, giving rise to {010} heteropolyhedral layers. Successive layers are then connected through $T(2)O_4$ tetrahedra, forming a three-dimensional heteropolyhedral framework where there are two kinds of channels hosting the *A*(2)' and *A*(1) sites in eight-fold coordination (Fig. 5).

Cation sites

Six independent cation sites occur in badalovite. Arsenic is hosted at the *T*(1) and *T*(2) sites. The former has bond distances ranging between 1.678 to 1.685 Å, with <*T*(1)–O> distance of 1.682 Å whereas the *T*(2)–O bond distances vary between 1.660 and 1.690 Å, with <*T*(2)–O> distance of 1.677 Å (Table 5). These values are in agreement with those reported by Pekov *et al*. (2020a) for badalovite and can be compared with the value of 1.685 Å reported by Majzlan *et al*. (2014) for the average <As–O> distance. The slight contraction can be related to the partial replacement of As by P. Considering the average <P–Φ> distance of 1.537 Å (Huminicki and Hawthorne, 2002), the observed values would point to the site occupancies $(As_{0.98}P_{0.02})$ and $(As_{0.95}P_{0.05})$ for *T*(1) and *T*(2), respectively. These are the site occupancies fixed during the crystal structure refinement. The BVS at the *T*(1) and *T*(2) sites is 5.00 and 5.06 valence units (v.u.), respectively.

The *M*(1) site is octahedrally coordinated and has a refined site occupancy $(Mg_{0.71}Mn_{0.29})$, corresponding to a mean atomic number (MAN) of 15.77 electrons. On the basis of electron

https://doi.org/10.1180/mgm.2025.8 Published online by Cambridge University Press

microprobe data, the site population ($Mg_{0.65}Mn_{0.25}Ca_{0.10}$) may be proposed, corresponding to a MAN of 16.05 electrons. Bond distances range between 2.155 and 2.189 Å, with an average <*M*(1)–O> distance of 2.172 Å. This value can be compared with that calculated using the proposed site population and the ionic radii given by Shannon (1976), i.e., 2.156 Å. The BVS at the *M*(1) site, calculated assuming such a population, is 1.94 v.u.

The *M*(2) site is bonded to 6 O atoms in octahedral coordination. Its refined site occupancy is ($Mg_{0.52}Fe_{0.48}$), corresponding to MAN = 18.72 electrons. Considering the results of chemical analysis, the site occupancy ($Mg_{0.55}Fe_{0.42}Zn_{0.02}Al_{0.01}$) can be proposed, corresponding to a MAN of 18.25 electrons. Bond distances range between 1.973 to 2.169 Å, with an average <*M*(2)–O> distance of 2.057 Å. This value can be compared with those calculated using the ionic radii of Shannon (1976), i.e., 2.060 Å. The BVS calculated at the *M*(2) site is 2.41 v.u., agreeing with the mixed (Mg^{2+}/Fe^{3+}) nature of its occupancy.

The *A*(1) and *A*(2)' sites are eight-fold coordinated. The *A*(1) site was refined as a mixed (Na,Ca) position, with the refined site occupancy ($Na_{0.65}Ca_{0.35}$); on the contrary, *A*(2)' was refined as a pure Na position. The *A*(1)–O and *A*(2)'–O bonds range from 2.358 to 2.962 Å and from 2.447 and 2.945 Å, respectively. The <*A*(1)–O> and <*A*(2)'–O> average distances are of 2.562 and 2.706 Å, respectively. Minor K could be hosted at the larger *A*(2)' site. Bond valence sums at the *A*(1) and *A*(2)' sites, calculated with the site occupancy of ($Na_{0.65}Ca_{0.35}$) and ($Na_{0.99}K_{0.01}$), respectively, are of 1.40 and 0.84 v.u.

Anion sites

Six independent O positions occur in badalovite, namely O(1)-O(6). All O atoms but that hosted at O(5) are four-fold coordinated; the O atom at O(5) is three-fold coordinated by two atoms hosted at the *M*(2) site and one tetrahedrally-coordinated cation at *T*(2). The BVS values of these O atoms range between 1.91 and 2.06 v.u., thus confirming that all anion positions are occupied by O^{2-} ions.

Structural formula of badalovite

Considering site multiplicity and the proposed site populations, the crystal chemical formula of badalovite from the Monte Calvario quarry can be written as $^{A(1)}(Na_{0.65}Ca_{0.35})\,^{A(2)'}(Na_{0.99}K_{0.01})^{M(1)}(Mg_{0.65}Mn_{0.25}Ca_{0.10})^{M(2)}(Mg_{0.55}Fe_{0.42}Zn_{0.02}Al_{0.01})_2{}^{T(1)+T(2)}(As_{2.88}P_{0.12})O_{12}$ (Z = 4).

Comparison between badalovite from Italy and Russia

A comparison between this new identification and the type material described by Pekov *et al*. (2020a) can be interesting. Chemical data of badalovite from Sicily show a distinct enrichment in Mn with respect to type badalovite, i.e., 0.27 *vs*. 0.02 apfu in the Italian and Russian sample, respectively. Moreover, a minor enrichment in Ca (0.30 *vs*. 0.20 apfu) and P (0.11 *vs*. 0.03 apfu) was found in the sample from the Monte Calvario quarry. The main consequence of this chemical variability is the detectable expansion of the unit-cell volume observed in the Sicilian badalovite, i.e., 941.6 $Å^3$ *vs*. 936.6 $Å^3$, with a ΔV = +0.53%. This volume increase seems to be related only to the lengthening of the *a* parameter, whereas the *b* and *c* parameters do not seem to be significantly affected by this chemical changes. The volume increase is in accord with the replacement of Mg^{2+} (ionic radius *r* = 0.720 Å –

https://doi.org/10.1180/mgm.2025.8 Published online by Cambridge University Press

Shannon, 1976) in octahedral environment with larger Mn^{2+} (r = 0.83 Å) and Ca^{2+} (r = 1.00 Å). Probably, this replacement occurs at the *M*(1) site, which is actually expanded with respect to the Russian sample, with an average <*M*(1)–O> distance of 2.172 Å, larger than the corresponding value in badalovite from Tolbachik, i.e., 2.134 Å. It is worth noting that all geometrical features of the *M*(1)-centered octahedron are expanded, as shown in Figure 6 where a comparison of the *M*(1)-polyhedra in the Russian and Italian samples is given. On the contrary, the average distances observed for the other cation sites are in agreement with those reported for the Russian sample, supporting the key role played by the *M*(1) site in the observed unit-cell expansion.

Remarks on the genesis of badalovite from Biancavilla

The second world occurrence of members of the badalovite-calciojohillerite series deserves further discussion. Indeed, these two minerals have been so far endemic of the Arsenatnaya fumarole at the Second scoria cone of the Northern Breakthrough of the Great Tolbachik Fissure Eruption, Tolbachik volcano, Kamchatka, Russia (Pekov *et al*., 2020a, 2021). Pekov *et al*. (2018) stressed the occurrence of H-free, (Mg,Na,Ca)-bearing arsenates in the deep zones of the fumaroles. There, alluaudite-supergroup minerals were useful to understand the geochemical gradients within the fumaroles. Calciojohillerite and badalovite were found only in the deepest sectors of the Arsenatnaya fumarole and, in particular, in the zone IIIb of Pekov *et al*. (2018), along with major hematite and fluorophlogopite and minor svabite and tilasite.

The mineral assemblage described at the Monte Calvario quarry reminds to the mineral association described by Pekov *et al*. (2018). Indeed, badalovite and calciojohillerite are associated with hematite, and in the same altered volcanic rocks abundant fluorophlogopite has been identified. Moreover, Gianfagna *et al*. (2014) described the As-enrichment in fluorapatite, with $As/(As+P+Si+S)_{at.}$ = 0.212, pointing to a solid solution with svabite, ideally $Ca_5(AsO_4)_3F$. As for the Arsenatnaya fumarole, the mineral assemblage from Monte Calvario points to high fO_2 conditions, low (atmospheric) pressure, and $T \geq 450$°C, in agreement with the measurements of Pekov *et al*. (2018).

Pekov *et al*. (2018) pointed out that the Arsenatnaya fumarole is an unusual kind of arsenate mineralization. Indeed, only some possible examples of fossil analogues are known. For instance, some arsenates were described from fissures of rhyolite and andesite (e.g., durangite – Wilson, 1986; maxwellite – Foord *et al*., 1991) and a member of the alluaudite supergroup, nickenichite, was first found at Nickenich, in the Eifel volcanic region, Germany (Auernhammer *et al*., 1993). The Monte Calvario quarry can be added to this short list of fumarolic arsenate mineralization.

Conclusions

The finding of intermediate members of the badalovite-calciojohillerite series allowed to highlight the structural flexibility of alluaudite-supergroup minerals, with the possible replacement of Mg^{2+} by Mn^{2+} and Ca^{2+} at octahedral positions. In addition to this crystal-chemical data, this work suggests that the Monte Calvario quarry could represent a fossil analogue of the exceptional kind of arsenate mineralization associated with fumarolic

https://doi.org/10.1180/mgm.2025.8 Published online by Cambridge University Press

environments accurately described by Pekov *et al*. (2018) from the currently active Arsenatnaya fumarole. In particular, the mineral assemblage of Monte Calvario seems to be characteristic of the deepest portion of the fumarole system. Considering the wide mineralogical variability of the arsenates assemblage from Tolbachik, more studies on the altered benmoreitic outcrops in the Biancavilla area as well as in others analogue localities of the Etna volcanic complex (e.g., Scordari *et al*., 2013) seem to be mandatory. These investigations would be able not only to give a better knowledge of the mineralogy of fumaroles of the Etna volcanic complex, but also to favour an improvement in our understanding of the possible dispersion of As and other potentially toxic elements in this sector of Sicily. Indeed, whereas Mazziotti-Tagliani *et al*. (2012) discussed the potential role of As-rich fluorapatite in the dispersion of As, the current study suggests that other hitherto unknown arsenate assemblages may occur in the Etnean region.

Acknowledgements

D.M. wishes to thank the mineral collector G. Sicurella for making available the studied specimen. The Centro per l'Integrazione della Strumentazione scientifica dell'Università di Pisa (CISUP) is acknowledged for the access to the CISUP X-ray Laboratory. The study of chemical composition was supported by the Ministry of Culture of the Czech Republic (long-term project DKRVO 2024-2028/1.II.b; National Museum, 00023272) for J.S. and Z.D. The authors wish to thanks the two anonymous reviewer for their useful revision.

References

Andreozzi G.B., Ballirano P., Gianfagna A., Mazziotti-Tagliani S. and Pacella, A. (2009) Structural and spectroscopic characterization of a suite of fibrous amphiboles with high environmental and health relevance from Biancavilla (Sicily, Italy). *American Mineralogist*, **94**, 1333–1340.

Auernhammer M., Effenberger H., Hentschel G., Reinnecke T. and Tillmanns E. (1993) Nickenichite, a new arsenate from Eifel, Germany. *Mineralogy and Petrology*, **48**, 153–166.

Burragato F., Comba P., Baiocchi V., Palladino D.M., Simei S., Gianfagna A., Paoletti L. and Pasetto R. (2005) Geo-volcanological, mineralogical and environmental aspects of quarry materials related to pleural neoplasm in the area of Biancavilla, Mount Etna (Eastern Sicily, Italy). *Environmental Geology*, **47**, 855–868.

Bruker AXS Inc. (2022) APEX4. Bruker Advanced X-ray Solutions, Madison, Wisconsin, USA.

Ercit T.S. (1993) Caryinite revisited. *Mineralogical Magazine*, **57**, 721–727

Foord E.E., Hlava P.F., Fitzpatrick J.J., Erd R.C. and Hinton R.W. (1991) Maxwellite and squawcreekite, two new minerals from the Black Range tin district, Catron County, New Mexico, U.S.A. *Neues Jahrbuch für Mineralogie, Monatshefte*, **1991**, 363–384.

Gagné O.C. and Hawthorne F.C. (2015) Comprehensive derivation of bond-valence parameters for ion pairs involving oxygen. *Acta Crystallographica*, **B71**, 562–578.

Gianfagna A. and Oberti R. (2001) Fluoro-edenite from Biancavilla (Catania, Sicily, Italy): Crystal chemistry of a new amphibole end-member. *American Mineralogist*, **86**, 1489–1493.

https://doi.org/10.1180/mgm.2025.8 Published online by Cambridge University Press

Gianfagna A., Scordari F., Mazziotti-Tagliani S., Ventruti G. and Ottolini L. (2007a) Fluorophlogopite from Biancavilla (Mt. Etna, Sicily, Italy): Crystal structure and crystal chemistry of a new F-dominant analog of phlogopite. *American Mineralogist*, **92**, 1601–1609.

Gianfagna A., Andreozzi G.B., Ballirano P. and Mazziotti-Tagliani S. (2007b) Structural and chemical contrasts between prismatic and fibrous fluoro-edenite from Biancavilla, Sicily, Italy. *The Canadian Mineralogist*, **45**, 249–262.

Gianfagna A., Mazziotti-Tagliani S., Croce A., Allegrina M. and Rinaudo C. (2014) As-rich apatite from Mt. Calvario: characterization by micro-Raman spectroscopy. *The Canadian Mineralogist*, **52**, 799–808.

Hatert F. (2019) A new nomenclature scheme for the alluaudite supergroup. *European Journal of Mineralogy*, **31**, 807–822.

Huminicki D.M.C. and Hawthorne F.C. (2002) The crystal chemistry of the phosphate minerals. *Reviews in Mineralogy and Geochemistry*, **48**, 123–253.

Koshlyakova N.N., Pekov I.V., Belakovskiy D.I., Vigasina M.F., Zubkova N.V., Agakhanov A.A., Britvin S.N., Sidorov E.G. and Pushcharovsky D.Y. (2020) Manganobadalovite, IMA 2020-035. CNMNC Newsletter No. 57. *Mineralogical Magazine*, **84**, 791–794.

Koshlyakova N.N., Pekov I.V., Belakovskiy D.I., Vigasina M.F., Zubkova N.V., Agakhanov A.A., Britvin S.N., Sidorov E.G. and Pushcharovsky D.Y. (2021) Calciohatertite, IMA 2021-013. CNMNC Newsletter 62. *Mineralogical Magazine*, **85**, 634–638.

Koshlyakova N.N., Pekov I.V., Agakhanov A.A., Bullock E., Belakovskiy D.I., Zubkova N.V., Chukanov N.V., Britvin S.N., Bulakh M.O., Burns P.C., Hazen R.M. and Zhitova E.S. (2024) Manganohatertite, IMA 2023-098. CNMNC Newsletter 77. *Mineralogical Magazine*, **88**, 203–209.

Krivovichev S.V., Vergasova L.P., Filatov S.K., Rybin D.S., Britvin S.N. and Ananiev V.V. (2013) Hatertite, $Na_2(Ca,Na)(Fe^{3+},Cu)_2(AsO_4)_3$, a new alluaudite-group mineral from Tolbachik fumaroles, Kamchatka peninsula, Russia. *European Journal of Mineralogy*, **25**, 683–691.

Majzlan J., Drahota P. and Filippi M. (2014) Parageneses and crystal chemistry of arsenic minerals. *Reviews in Mineralogy & Geochemistry*, **79**, 17–184.

Mazziotti-Tagliani S., Angelone M., Armiento G., Pacifico R., Cremisini C. and Gianfagna A. (2012) Arsenic and fluorine in the Etnean volcanics from Biancavilla, Sicily, Italy: environmental implications. *Environmental Earth Science*, **66**, 561–572.

Pekov I.V., Lykova I.S., Koshlyakova N.N., Belakovskiy D.I., Vigasina M.F., Agakhanov A.A., Britvin S.N., Turchkova A.G., Sidorov E.G. and Giester G. (2016) Magnesiohatertite, IMA 2016-078. CNMNC Newsletter No. 34, December 2016, page 1319. *Mineralogical Magazine*, **80**, 1315–1321.

Pekov I.V., Koshlyakova N.N., Zubkova N.V., Lykova I.S., Britvin S.N., Yapaskurt V.O., Agakhanov A.A., Shchipalkina N.V., Turchkova A.G. and Sidorov E.G. (2018) Fumarolic arsenates – a special type of arsenic mineralization. *European Journal of Mineralogy*, **30**, 305–322.

Pekov I.V., Koshlyakova N.N., Agakhanov A.A., Zubkova N.V., Belakovskiy D. I., Vigasina M. F., Turchkova A.G., Sidorov E.G. and Pushcharovsky D.Y. (2020a) New arsenate minerals from the Arsenatnaya fumarole, Tolbachik volcano, Kamchatka, Russia. XIV.

https://doi.org/10.1180/mgm.2025.8 Published online by Cambridge University Press

Badalovite, $NaNaMg(MgFe^{3+})(AsO_4)_3$, a member of the alluaudite group. *Mineralogical Magazine*, **84** 616–622.

Pekov I.V., Lykova I., Koshlyakova N.N., Belakovskiy D.I., Vigasina M.F., Turchkova A.G., Britvin S.N., Sidorov E.G. and Scheidl K.S. (2020b) A new mineral species zincobradaczekite, $NaCuCuZn_2(AsO_4)_3$, and a new isomorphous series bradaczekite-zincobradaczekite in the alluaudite group. *Physics and Chemistry of Minerals*, **47**, 36

Pekov I.V., Koshlyakova N.N., Agakhanov A.A., Zubkova N.V., Belakovskiy D. I., Vigasina M. F., Turchkova A.G., Sidorov E.G. and Pushcharovsky D.Y. (2021) New arsenate minerals from the Arsenatnaya fumarole, Tolbachik volcano, Kamchatka, Russia. XV. Calciojohillerite, $NaCaMgMg_2(AsO_4)_3$, a member of the alluaudite group. *Mineralogical Magazine*, **85**, 215–223.

Pekov I.V., Koshlyakova N.N., Belakovskiy D.I., Vigasina M.F., Zubkova N.V., Agakhanov A.A., Britvin S.N., Sidorov E.G. and Pushcharovsky D.Y. (2022a) New arsenate minerals from the Arsenatnaya fumarole, Tolbachik volcano, Kamchatka, Russia. XVIII. Khrenovite, $Na_3Fe^{3+}{}_2(AsO_4)_3$, the member with the highest sodium in the alluaudite supergroup. *Mineralogical Magazine*, **86**, 897–902.

Pekov I.V., Koshlyakova N.N, Belakovskiy D.I., Vigasina M.F., Zubkova N.V., Agakhanov A.A., Britvin S.N., Sidorov E.G. and Pushcharovsky D.Y. (2022b) New arsenate minerals from the Arsenatnaya fumarole, Tolbachik volcano, Kamchatka, Russia. XVII. Paraberzeliite, $NaCaCaMg_2(AsO_4)_3$, an alluaudite-group member dimorphous with berzeliite. *Mineralogical Magazine*, **86**, 103–111.

Pouchou J.L. and Pichoir F. (1985) "PAP" ($\phi\rho Z$) procedure for improved quantitative microanalysis. Pp. 104–106 in: Microbeam Analysis (J.T. Armstrong, editor). San Francisco Press, San Francisco.

Scordari F., Schingaro E., Ventruti G., Nicotra E., Viccaro M. and Mazziotti-Tagliani S. (2013) Fluorophlogopite from Piano delle Concazze (Mt. Etna, Italy): Crystal chemistry and implications for the crystallization conditions. *American Mineralogist*, **98**, 1017–1025.

Sejkora J., Plášil J., Čejka J., Dolníček Z. and Pavlíček R. (2020) Molecular structure of the arsenate mineral chongite from Jáchymov – a vibrational spectroscopy study. *Journal of Geosciences*, **65**, 111–120.

Shannon R.D. (1976) Revised effective ionic radii and systematic studies of interatomic distances in halides and chalcogenides. *Acta Crystallographica*, **A32**, 751–767.

Sheldrick G.M. (2015) Crystal structure refinement with SHELXL. *Acta Crystallographica*, **C71**, 3–8.

Sicurella G., Ciriotti M.E., Gianfagna A., Mazziotti-Tagliani S. and Blass G. (2010) Minerali di Monte Calvario, Biancavilla, (Catania, Sicilia). *Micro*, 329–368.

Tait K.T. and Hawthorne F.C. (2003) Refinement of the crystal structure of arseniopleite: confirmation of its status as a valid species. *The Canadian Mineralogist*, **41**, 71–77.

Tait K.T., Hawthorne F.C. and Halden N.M. (2021) Alluaudite-group phosphate and arsenate minerals. *The Canadian Mineralogist*, **59**, 243–263.

Wilson, A.J.C. (1992) International Tables for Crystallography. Volume C: Mathematical, Physical and Chemical Tables. Kluwer Academic Publishers, Dordrecht, The Netherlands.

https://doi.org/10.1180/mgm.2025.8 Published online by Cambridge University Press

Wilson, W.E. (1986) Durangite from Utah. *Mineralogical Record*, **17**, 342.

Wojdyr, M. (2010) Fityk: a general-purpose peak fitting program. *Journal of Applied Crystallography*, **43**, 1126–1128.

https://doi.org/10.1180/mgm.2025.8 Published online by Cambridge University Press

Table captions

Table 1. Electron microprobe data for alluaudite-group minerals from the Monte Calvario quarry.

Table 2. Raman bands (in cm^{-1}) and band assignments of badalovite from Monte Calvario quarry compared with those of badalovite and calciojohillerite from the Arsenatnaya fumarole, Tolbachik volcano, Kamchatka, Russia.

Table 3. Summary of crystal data and parameters describing data collection and refinement for badalovite from the Monte Calvario quarry.

Table 4. Sites, Wyckoff site, site occupancy factors (s.o.f.), fractional atom coordinates and equivalent isotropic displacement parameters ($Å^2$) for badalovite from the Monte Calvario quarry.

Table 5. Selected bond distances (Å) for badalovite from the Monte Calvario quarry.

Table 6. Weighted bond-valence sums (in valence units, v.u.) for badalovite from the Monte Calvario quarry.

Figure captions

Fig. 1. Badalovite, aggregates of prismatic crystal associated with black tabular crystals of hematite. Monte Calvario quarry, Biancavilla, Etna volcanic complex, Sicily, Italy. Private collection, photo D. Mauro.

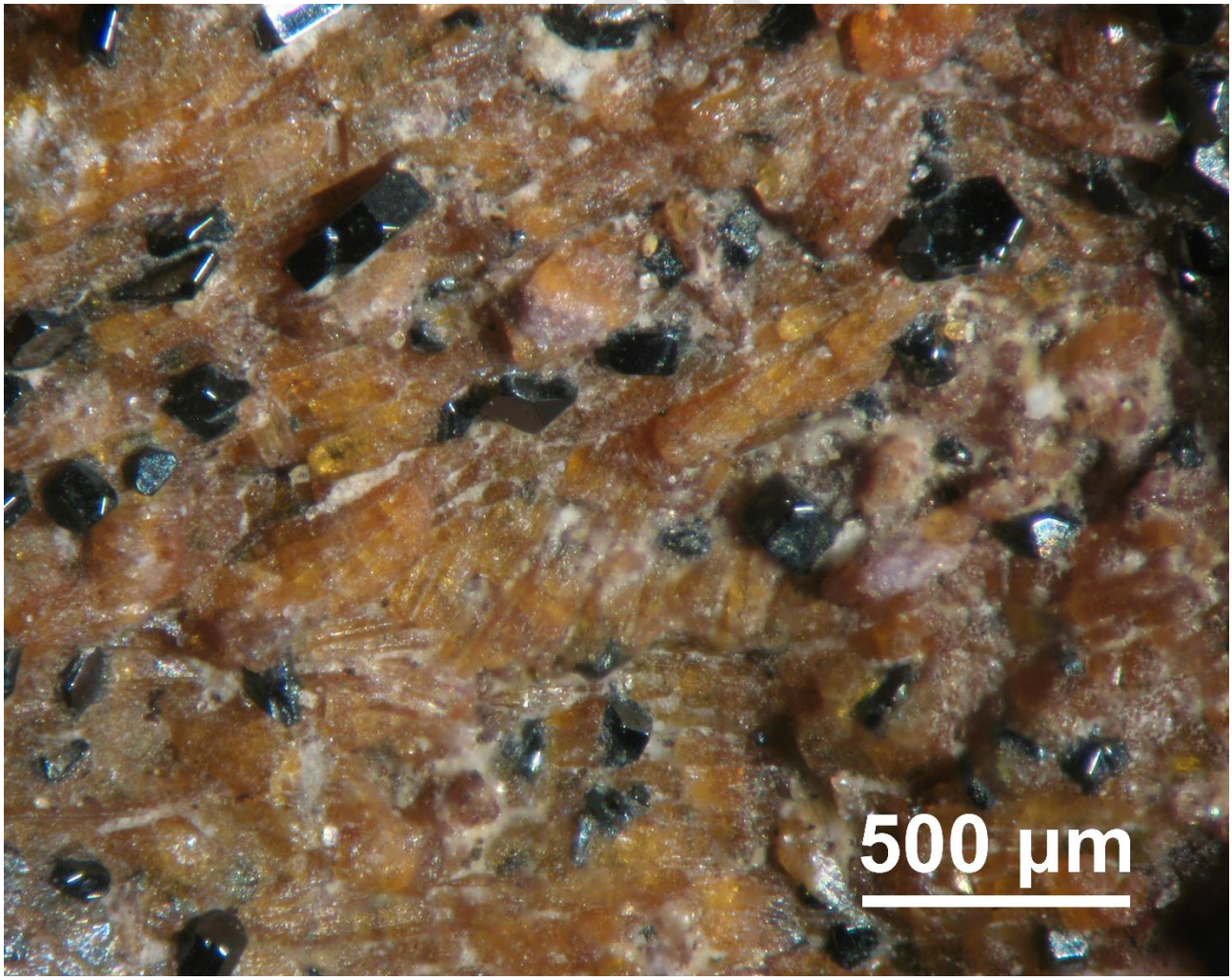

https://doi.org/10.1180/mgm.2025.8 Published online by Cambridge University Press

Fig. 2. X-ray maps showing Ca, Fe, Mg and Na distribution and the position of the spot analyses for the studied sample.

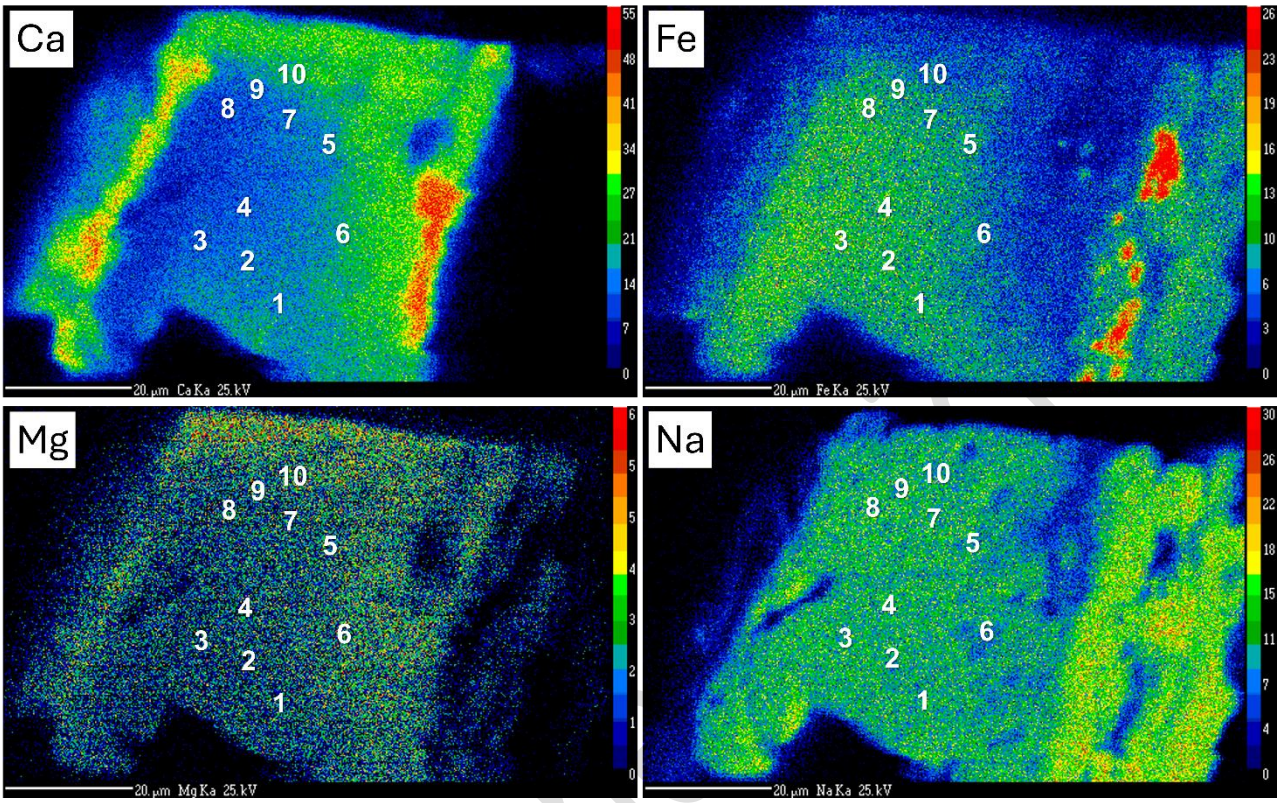

https://doi.org/10.1180/mgm.2025.8 Published online by Cambridge University Press

Fig. 3. Relations between the atomic ratios $M^{2+}/\Sigma M$ and $A^{+}/\Sigma A$ for the studied sample (red triangles). For the sake of clarity, the positions of the ideal compositions of badalovite (orange square), calciojohillerite (light blue square), and the intermediate member between these two species (green square) are shown. Roman numbers indicate the three different chemical domains.

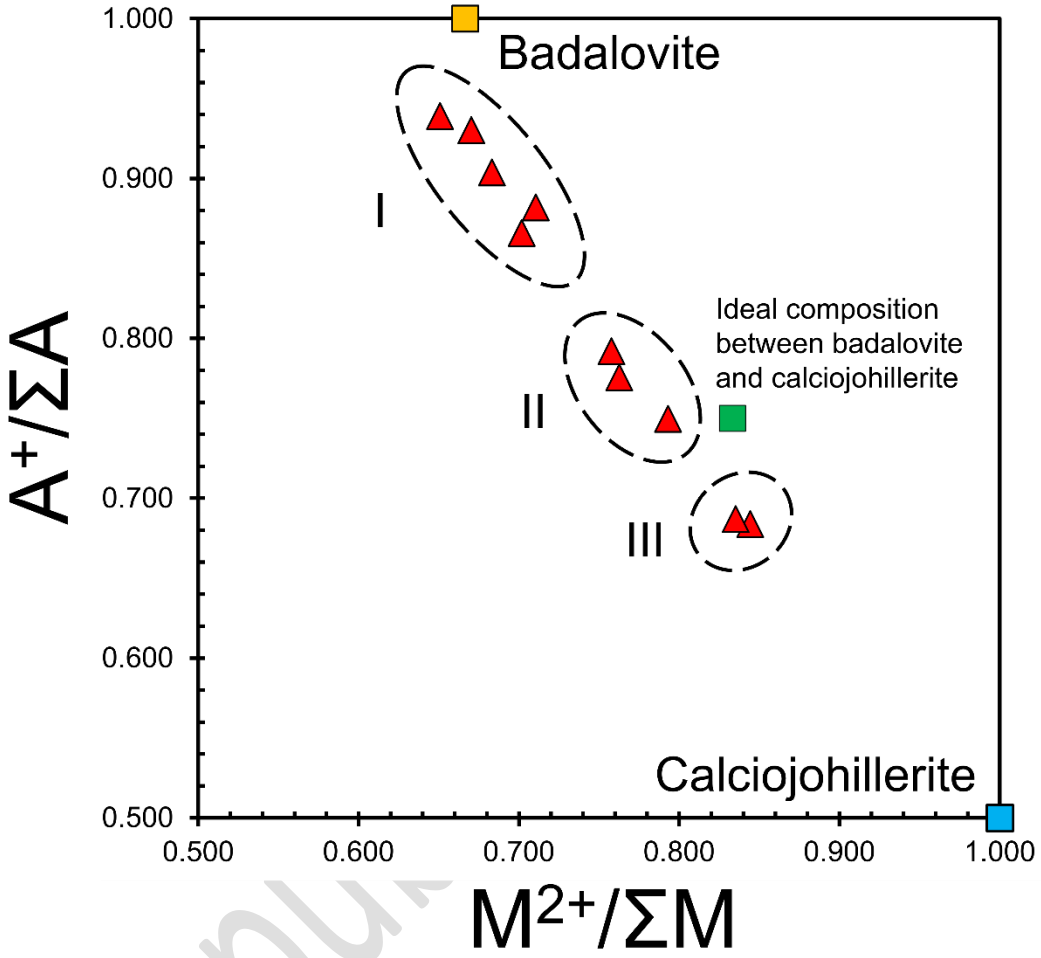

https://doi.org/10.1180/mgm.2025.8 Published online by Cambridge University Press

Fig. 4. Raman spectrum, in the range between 100–1300 cm^{-1}, and band positions of badalovite from the Monte Calvario quarry.

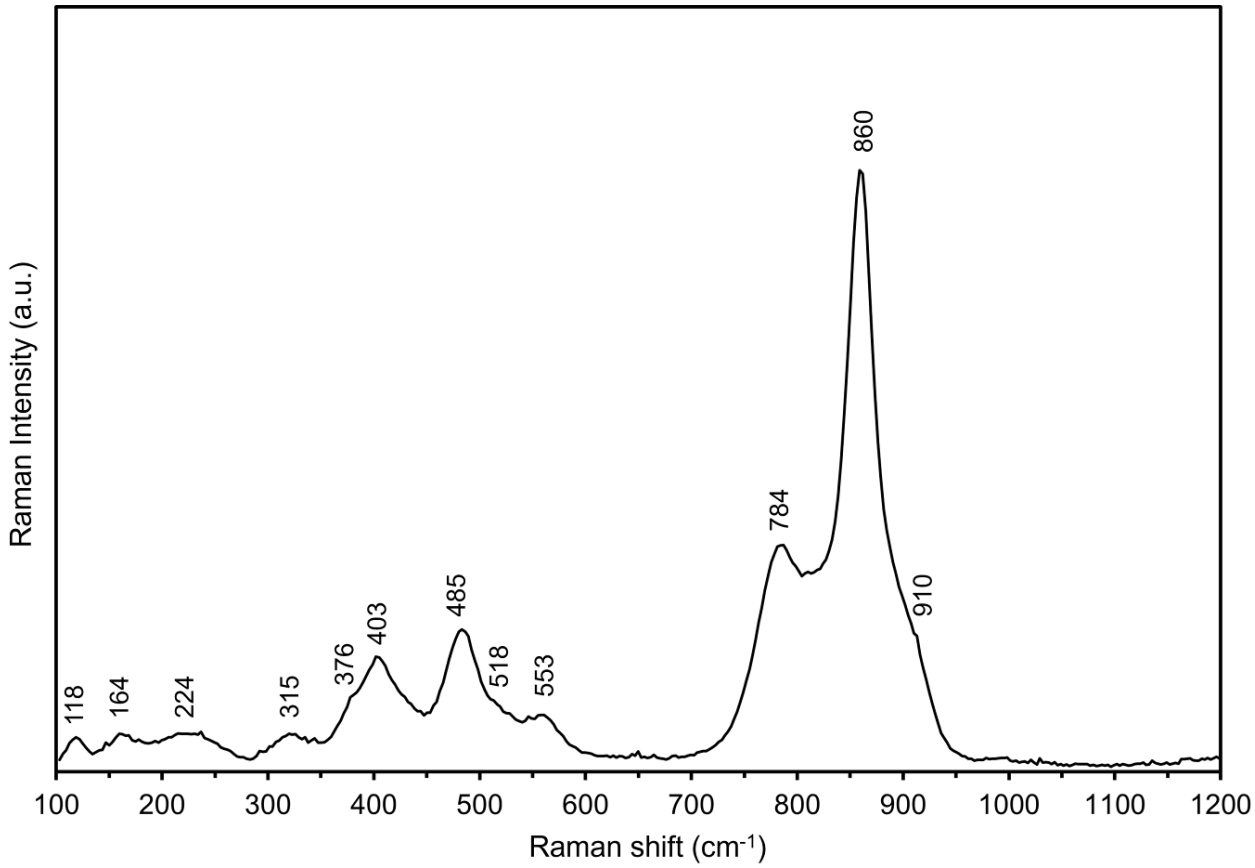

https://doi.org/10.1180/mgm.2025.8 Published online by Cambridge University Press

Fig. 5. Details of the crystal structure of badalovite. (a) The octahedral chains running along [10-1], with $M(2)_2O_{10}$ dimers (in green) connected through $M(1)$-centered octahedra (yellow). (b) The heteropolyhedral layer formed by octahedral chains interconnected through $T(1)O_4$ tetrahedra (red), as seen down **b**. (c) The crystal structure as seen down **c**. The heteropolyhedral layers are connected through $T(2)O_4$ tetrahedra, forming a framework hosting $A(1)$ and $A(2)'$ sites (grey circles).

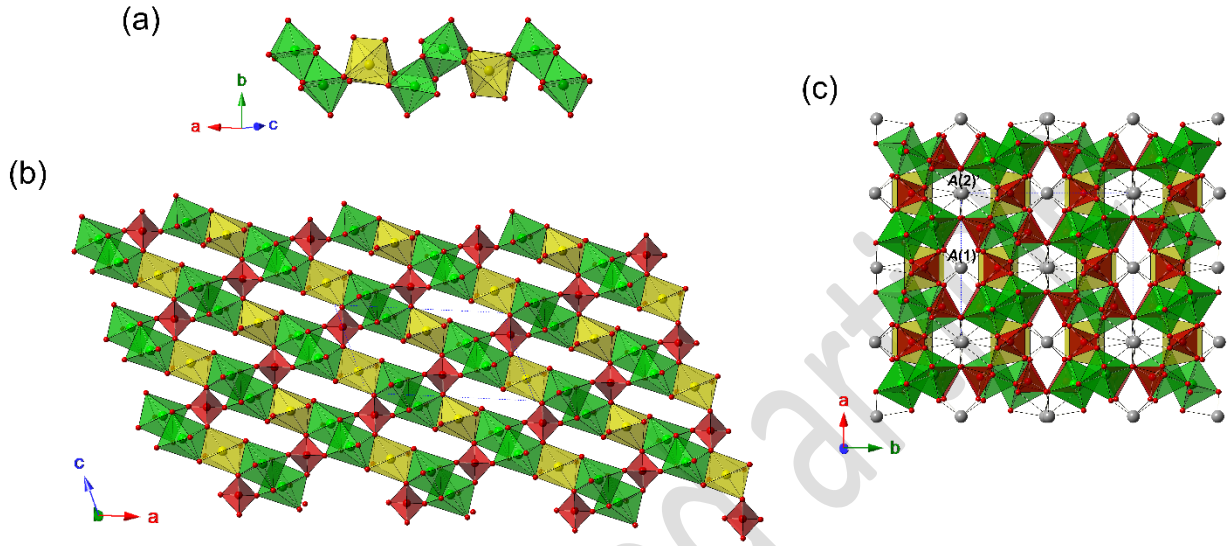

Fig. 6. Comparison between the $M(1)$-centered octahedron in badalovite from Tolbachik (on left) and Sicily (on right). Selected values of O···O distances are given in Å.

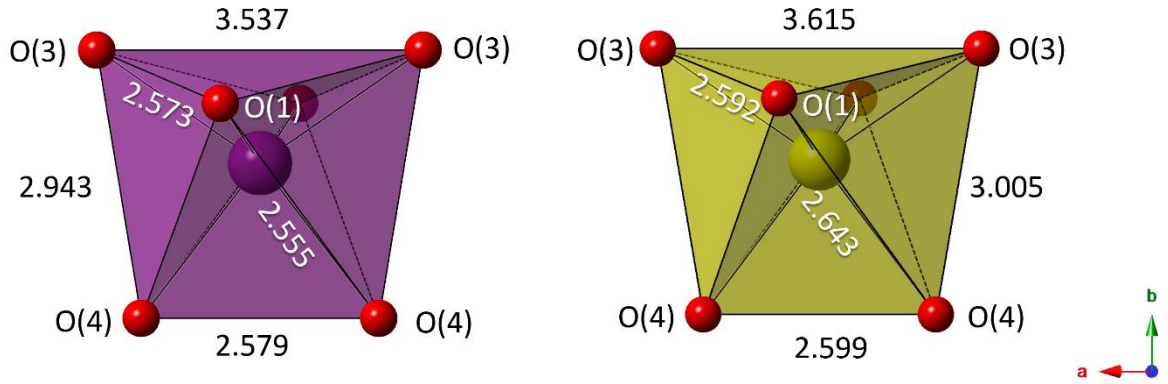

https://doi.org/10.1180/mgm.2025.8 Published online by Cambridge University Press

Table 1. Electron microprobe data for alluaudite-group minerals from the Monte Calvario quarry.

	Domain I					Domain II			Domain III	
Oxide (in wt%)	1	2	3	4	5	6	7	8	9	10
SO_3	0.05	0.05	-	0.04	-	0.06	-	0.01	0.09	0.07
P_2O_5	2.15	1.91	1.83	2.44	2.56	3.15	3.14	3.76	2.88	3.45
As_2O_5	57.21	57.37	56.73	57.06	58.82	57.51	57.03	55.83	57.52	56.17
Al_2O_3	0.15	0.18	0.20	0.19	0.22	0.09	0.01	-	-	0.05
Fe_2O_3	11.76	12.82	13.97	12.15	13.29	8.72	9.82	10.22	6.68	7.08
MgO	11.19	10.56	9.74	11.96	11.21	15.10	13.93	14.15	16.30	16.11
CaO	4.33	3.85	3.27	3.69	2.73	5.24	4.87	4.40	6.58	6.60
MnO	3.65	3.58	3.47	3.23	2.95	3.36	3.40	3.25	3.40	3.52
ZnO	0.32	0.48	0.44	0.54	0.27	0.27	0.29	0.31	0.13	0.14
Na_2O	9.54	9.56	9.89	9.57	10.07	8.64	8.74	9.24	7.82	7.69
K_2O	0.09	0.05	0.09	0.05	0.06	0.05	0.04	0.02	0.07	0.06
Total	100.43	100.41	99.06	100.92	100.18	102.20	101.37	101.28	101.47	101.15
Element (apfu)										
A-chemical constituents										
Na	1.78	1.79	1.87	1.77	1.88	1.57	1.60	1.70	1.42	1.46
K	0.01	0.01	0.01	0.01	0.01	0.01	0.01	0.00	0.01	0.01
Ca	0.24	0.19	0.11	0.27	0.13	0.53	0.46	0.45	0.66	0.67
Σ A constituents	2.03	1.99	1.99	2.05	2.02	2.11	2.07	2.15	2.09	2.14
M-chemical constituents										
Mg	1.60	1.52	1.41	1.70	1.61	2.11	1.97	2.00	2.28	2.26
Mn	0.30	0.29	0.29	0.26	0.24	0.27	0.27	0.26	0.27	0.28
Ca	0.21	0.21	0.23	0.11	0.15	0.00	0.03	0.00	0.00	0.00
Zn	0.02	0.03	0.03	0.04	0.02	0.02	0.02	0.02	0.01	0.01
Fe^{3+}	0.85	0.93	1.02	0.87	0.96	0.61	0.70	0.73	0.47	0.50
Al	0.02	0.02	0.02	0.02	0.02	0.01	0.01	0.00	0.00	0.01
Σ M constituents	3.00	3.00	3.00	3.00	3.00	3.02	3.00	3.01	3.03	3.06
T-chemical constituents										
As	2.88	2.89	2.89	2.85	2.86	2.81	2.82	2.77	2.82	2.77
P	0.09	0.08	0.08	0.10	0.10	0.12	0.13	0.15	0.11	0.14
S	0.01	0.01	0.00	0.00	0.00	0.01	0.00	0.01	0.01	0.01
Σ T constituents	2.98	2.98	2.97	2.95	2.96	2.94	2.95	2.93	2.94	2.92

Note = apfu, atom per formula unit.

https://doi.org/10.1180/mgm.2025.8 Published online by Cambridge University Press

Table 2. Raman bands (in cm^{-1}) and band assignments of badalovite from Monte Calvario quarry compared with those of badalovite and calciojohillerite from the Arsenatnaya fumarole, Tolbachik volcano, Kamchatka, Russia.

Badalovite (this study)	Badalovite (Pekov *et al*., 2020a)	Calciojohillerite (Pekov *et al*., 2021)	Assignments
118, 164, 224	207, 279	213	*A*–O, *M*–O and lattice modes
315, 376, 403, **485**, 518, 553	380, 422, **487**, *561*	325, 381, 426, **486**, *574*	v_2 and v_4 $(AsO_4)^{3-}$
784, **860**, 910	800, **862**, **915**	783, **861**, **896**	v_1 and v_3 $(AsO_4)^{3-}$

Note = in bold, the strongest Raman bands; in italic, the band positions interpreted as due to Fe–O vibration modes by Pekov *et al*. (2020a) and Pekov *et al*. (2021).

Table 3. Summary of crystal data and parameters describing data collection and refinement for badalovite from the Monte Calvario quarry.

Crystal data	
Crystal size (mm)	0.110 × 0.085 × 0.060
Cell setting, space group	Monoclinic, *C*2/*c*
a (Å)	11.9760(5)
b (Å)	12.7857(5)
c (Å)	6.6650(3)
β (°)	112.689(2)
V (Å^3)	941.58(7)
Z	4
Data collection and refinement	
Radiation, wavelength (Å)	Mo*K*α, λ = 0.71073
Temperature (K)	300(2)
Maximum observed 2θ (°)	65.05
Measured reflections	7084
Unique reflections	1711
Reflections $F_o > 4\sigma(F_o)$	1637
R_{int} after absorption correction	0.0233
Rσ	0.0201
Range of *h*, *k*, *l*	$-18 \le h \le 18$ $-19 \le k \le 17$ $-10 \le l \le 10$
R [F_o>4 σ F_o]	0.0257
R (all data)	0.0270
wR (on F_o^2)[1]	0.0563
Goodness of fit	1.277
Number of least-squares parameters	97
Maximum and minimum residual peak (*e*/Å^3)	0.81 [at 0.83 Å from O(6)] -0.80 [at 0.88 Å from O(1)]

[1] $w = 1/[\sigma^2(F_o^2)+8.3102P]$, where $P = (F_o^2+2F_c^2)/3$.

https://doi.org/10.1180/mgm.2025.8 Published online by Cambridge University Press

Table 4. Sites, Wyckoff site, site occupancy factors (s.o.f.), fractional atom coordinates and equivalent isotropic displacement parameters (Å^2) for badalovite from the Monte Calvario quarry.

Site	Wyckoff site	*s.o.f.*	*x*/*a*	*y*/*b*	*z*/*c*	$U_{iso/eq}$
A(1)	4*b*	$Na_{0.653(15)}Ca_{0.347(15)}$	½	0	0	0.0234(6)
A(2)'	4*e*	$Na_{1.00}$	0	-0.0093(3)	¼	0.0397(6)
M(1)	4*e*	$Mg_{0.710(7)}Mn_{0.290(7)}$	0	0.26572(8)	¼	0.0106(3)
M(2)	8*f*	$Mg_{0.516(5)}Fe_{0.484(5)}$	0.28357(5)	0.65677(5)	0.37311(9)	0.00804(18)
T(1)	4*e*	$As_{0.98}P_{0.02}$	0	0.71369(3)	¼	0.00788(9)
T(2)	8*f*	$As_{0.95}P_{0.05}$	0.23526(3)	0.88924(2)	0.12400(5)	0.00787(7)
O(1)	8*f*	$O_{1.00}$	0.45961(19)	0.71218(18)	0.5241(3)	0.0127(4)
O(2)	8*f*	$O_{1.00}$	0.10789(19)	0.62906(18)	0.2536(4)	0.0155(4)
O(3)	8*f*	$O_{1.00}$	0.3368(2)	0.66920(17)	0.1181(3)	0.0119(4)
O(4)	8*f*	$O_{1.00}$	0.11728(19)	0.40019(18)	0.3166(4)	0.0141(4)
O(5)	8*f*	$O_{1.00}$	0.21975(19)	0.81715(17)	0.3242(3)	0.0111(4)
O(6)	8*f*	$O_{1.00}$	0.3338(2)	0.50481(17)	0.3924(4)	0.0143(4)

Table 5. Selected bond distances (Å) for badalovite from the Monte Calvario quarry.

A(1)	–O(2) ×2	2.359(2)	*M*(1)	–O(4) ×2	2.155(2)	*T*(1)	–O(2) ×2	1.678(2)
	–O(4) ×2	2.402(2)		–O(1) ×2	2.173(2)		–O(1) ×2	1.685(2)
	–O(4) ×2	2.534(2)		–O(3) ×2	2.188(2)		Average	1.682
	–O(2) ×2	2.954(2)		Average	2.172			
	Average	2.562				*T*(2)	–O(4)	1.660(2)
			M(2)	–O(2)	1.973(2)		–O(6)	1.676(2)
A(2)	–O(6) ×2	2.447(2)		–O(6)	2.023(2)		–O(3)	1.683(2)
	–O(6) ×2	2.521(2)		–O(3)	2.039(2)		–O(5)	1.690(2)
	–O(3) ×2	2.911(3)		–O(5)	2.060(2)		Average	1.677
	–O(1) ×2	2.945(4)		–O(1)	2.079(2)			
	Average	2.706		–O(5)	2.169(2)			
				Average	2.057			

https://doi.org/10.1180/mgm.2025.8 Published online by Cambridge University Press

Table 6. Weighted bond-valence sums (in valence units, v.u.) for badalovite from the Monte Calvario quarry.

Site	*A*(1)	*A*(2)'	*M*(1)	*M*(2)	*T*(1)	*T*(2)	Σ_{anions}	Theor.
O(1)		$^{2\times\downarrow}$0.05	$^{2\times\downarrow}$0.32	0.38	$^{2\times\downarrow}$1.24		1.99	2.00
O(2)	$^{2\times\downarrow}$0.25 $^{2\times\downarrow}$0.06			0.49	$^{2\times\downarrow}$1.26		2.06	2.00
O(3)		$^{2\times\downarrow}$0.06	$^{2\times\downarrow}$0.31	0.42		1.24	2.03	2.00
O(4)	$^{2\times\downarrow}$0.23 $^{2\times\downarrow}$0.16		$^{2\times\downarrow}$0.34			1.33	2.06	2.00
O(5)				0.39 0.30		1.22	1.91	2.00
O(6)		$^{2\times\downarrow}$0.17 $^{2\times\downarrow}$0.14		0.43		1.27	2.01	
$\Sigma_{cations}$	1.40	0.84	1.94	2.41	5.00	5.06		
Theor.	1.35	1.00	2.00	2.43	5.00	5.00		

Note: left superscripts indicate the number of equivalent bonds involving anions. The following site occupancy were used for calculating the bond-valence sums: *A*(1) = $Na_{0.65}Ca_{0.35}$; *A*(2)' = $Na_{0.99}K_{0.01}$; *M*(1) = $Mg_{0.65}Mn_{0.25}Ca_{0.10}$; *M*(2) = $Mg_{0.55}Fe^{3+}_{0.42}Zn_{0.02}Al_{0.01}$; *T*(1) = $As_{0.98}P_{0.02}$; and *T*(2) = $As_{0.95}P_{0.05}$.

https://doi.org/10.1180/mgm.2025.8 Published online by Cambridge University Press